


# Prediction of Green Phosphorus with Tunable Direct Band Gap and High Mobility

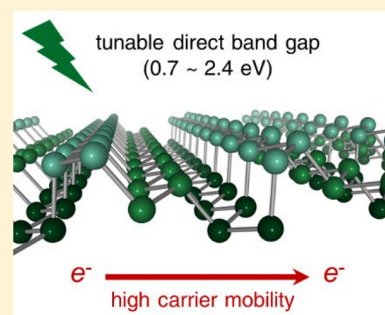
Woo Hyun Han,<sup>†</sup> Sunghyun Kim,<sup>†,§</sup> In-Ho Lee,<sup>‡</sup> and Kee Joo Chang<sup>\*,†,§</sup>

<sup>†</sup>Department of Physics, Korea Advanced Institute of Science and Technology, Daejeon 34141, Korea

<sup>‡</sup>Korea Research Institute of Standards and Science, Daejeon 34113, Korea

 Supporting Information

**ABSTRACT:** Black phosphorus is an emerging material in nanoelectronics and nanophotonics due to its high carrier mobility and anisotropic in-plane properties. In addition, the polymorphism of phosphorus leads to numerous searches for new allotropes that are more attractive than black phosphorus in a variety of applications. On the basis of *ab initio* evolutionary crystal structure search computation, we report the prediction of a phosphorus allotrope called green phosphorus ( $\lambda$ -P), which exhibits direct band gaps ranging from 0.7 to 2.4 eV and strong anisotropy in optical and transport properties. Free-energy calculations show that a single-layer form, termed green phosphorene, is energetically more stable than blue phosphorene, and a phase transition from black to green phosphorene can occur at temperatures above 87 K. We suggest that green phosphorene can be synthesized on corrugated metal surfaces rather than clean surfaces due to its buckled structure, providing guidance to achieving epitaxial growth.



The successful isolation of graphene,<sup>1</sup> a single layer of carbon atoms in a 2D honeycomb lattice, has generated tremendous interest in 2D layered materials.<sup>2</sup> Various applications using graphene have been explored based on its unusual properties such as massless Dirac fermions, high mobility, and high thermal conductivity.<sup>3,4</sup> However, the gapless nature of graphene has been an obstacle in practical applications for electronic devices because of its low on/off ratios.<sup>5</sup> Transition-metal dichalcogenides belonging to the family of 2D materials have semiconducting gaps in the visible range, but the carrier mobility in thin films is significantly reduced.<sup>6</sup> Recently, atomically thin black phosphorus has been successfully separated from its layered bulk,<sup>7,8</sup> and this emerging 2D material with a tunable band gap by varying the number of atomic layers bridges the gap between graphene and transition-metal dichalcogenides.<sup>9,10</sup> Because of its high anisotropic mobility, black phosphorus is considered to be a promising material for electronic and optoelectronic devices.<sup>6–8,11,12</sup>

Elemental phosphorus is known to exist in several 3D allotropes, such as red, white, and violet phosphorus, in addition to black phosphorus ( $\alpha$ -P), which is the most stable phase among them. Because of the presence of various phases, it is expected that an unknown phosphorus allotrope will form under the control of substrate, temperature, and pressure. Zhu and Tománek proposed a new stable phase of phosphorus called blue phosphorus ( $\beta$ -P), with structural similarity to buckled graphene.<sup>13</sup> Unlike black phosphorus, blue phosphorus displays indirect band gaps, regardless of the number of atomic layers. Other 2D structures such as  $\gamma$ -,  $\delta$ -,  $\epsilon$ -,  $\zeta$ -,  $\eta$ -,  $\theta$ -, and  $\psi$ -phosphorene were later suggested based on theoretical calculations.<sup>14–18</sup> Recently, blue phosphorene has been

successfully synthesized on the Au(111) substrate by molecular beam epitaxy.<sup>19</sup> The realization of blue phosphorene not only opens up the potential of various metastable allotropes but also motivates research into a new level of phosphorus that provides exciting characteristics such as broad band gaps and high anisotropic mobility.

We report a new phosphorus allotrope called green phosphorus using an *ab initio* evolutionary crystal structure search method. The new P allotrope belongs to a class of 2D materials and has direct band gap characteristics in the range of 0.7–2.4 eV depending on the number of atomic layers. Because of the weak interlayer interaction, green phosphorus should be easily exfoliated to form thin films. A monolayer of green phosphorus exhibits high in-plane anisotropy in optical absorption and transport properties, which is suitable for novel applications in electronic and optical devices. We discuss the transition pathway from black to green phosphorene and the effects of temperature and substrate on the synthesis of green phosphorene.

For phosphorus systems with  $N$  atoms per unit cell ( $N = 2k$ ,  $3 \leq k \leq 12$ ), we explored low-energy allotropes by using an *ab initio* evolutionary crystal structure search method, as implemented in the AMADEUS code.<sup>20</sup> Distinct configurations were generated by employing the conformational space annealing algorithm for global optimization. We find that black phosphorus is the most stable allotrope at zero temperature, as reported previously.<sup>21</sup> Among various metastable configurations, we obtained a novel allotrope in the space

**Received:** August 16, 2017

**Accepted:** September 11, 2017

**Published:** September 11, 2017

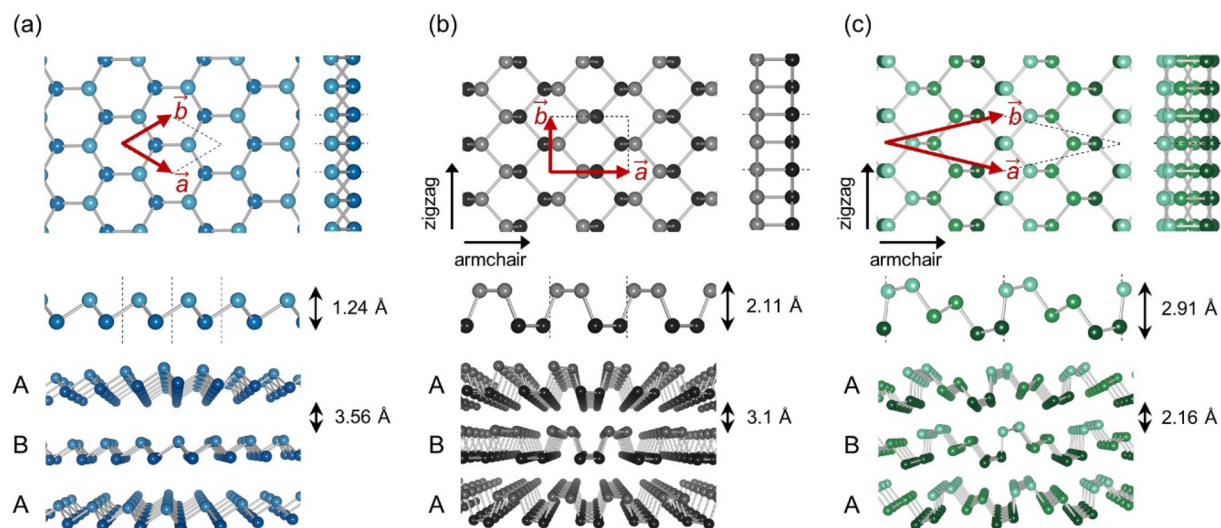


**Figure 1.** Top and side views of the atomic structures of (a)  $\beta$ -P (blue), (b)  $\alpha$ -P (black), and (c)  $\lambda$ -P (green) are compared. In upper panels,  $\vec{a}$  and  $\vec{b}$  represent the lattice vectors in a monolayer, and the atomic layers in AB stacking are shown in lower panels. Note that although green phosphorene consists of armchair and zigzag ridges on the side view, armchair and zigzag directions are defined in a manner similar to black phosphorene.

group  $C2/m$  (12), which contains six atoms in the primitive cell. The new metastable allotrope, termed green phosphorus ( $\lambda$ -P), has a layered structure like black and blue phosphorus (Figure 1).

Figure 1 illustrates the structural relationship between black, blue, and green phosphorus. Black and blue phosphorus exhibit distinct structural differences in side view, such as armchair and zigzag ridges, respectively. Because the zigzag ridges are less puckered, the layer thickness of blue phosphorus is reduced to 1.24 Å (compared with 2.11 Å layer thickness of black phosphorus). In black phosphorene, reversing all bonds in every fourth row from an up-position to a down-position (or vice versa) converts all armchair ridges to zigzag ridges, leading to the transformation to blue phosphorene (Figure 2a).<sup>13</sup> In green phosphorus, the AB stacking of atomic layers is energetically more favorable by 15 meV/atom than the AA stacking. All of the atoms are three-fold coordinated, with bond lengths of 2.23 and 2.26 Å for the in-plane and out-of-plane bonds, respectively. Because a monolayer of green phosphorus, termed green phosphorene, contains three slightly buckled atomic layers, it has the largest layer thickness (2.91 Å) among the three allotropes. Green phosphorene consists of armchair and zigzag ridges, and thus its structure is characterized by the combination of black and blue phosphorene (Figure 2b). The transformation from black to green phosphorene can be viewed by flipping every twelfth row of bonds from the up-position to the down-position by dislocations after every fourth row of the armchair ridges is reversed to the opposite side of the 2D plane.

Besides green phosphorus, we obtained other metastable configurations that can be viewed as a combination of black and blue phosphorus (Figure S1). In disorder phases, in which black and blue phosphorus segments are irregularly arranged, their stability may be enhanced by the increase in entropy. Irregular flipping of armchair and zigzag ridges tends to increase the structural energy by suppressing interlayer interactions because it creates highly corrugated atomic layers (Figure S1). Therefore, although various layered structures composed of black and blue phosphorus segments irregularly are possible, heavily puckered structures are not advantageous for forming layered structures in actual experiments.

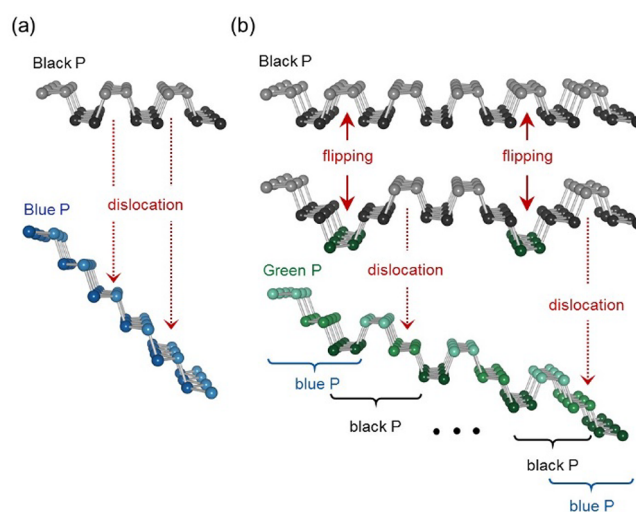


**Figure 2.** Schematic view of the structural transformations from  $\alpha$ -P (black) to (a)  $\beta$ -P (blue) and to (b)  $\lambda$ -P (green). (a) Blue phosphorene can be converted from black phosphorene after reversing all bonds in every fourth row. (b) On the contrary, black phosphorene transforms to green phosphorene via an intermediate structure formed by flipping every fourth row of the armchair ridges, followed by introducing dislocations that flip every twelfth row of bonds from an up-position to a down-position.

The lattice parameters and energetics of black, blue, and green phosphorus are compared in Table 1. Green phosphorus is more stable by 67 meV/atom than blue phosphorus, while its energy is higher by 19 meV/atom than that of black phosphorus. The monoclinic  $C2/m$  structure of green phosphorus has the equilibrium lattice parameters of  $a = 10.492$  Å,  $b = 3.312$  Å,  $c = 7.894$  Å,  $\alpha = 90^\circ$ ,  $\beta = 59.44^\circ$ , and  $\gamma = 90^\circ$  as well as three inequivalent Wyckoff positions of  $4i$  (0.768, 0, 0.893),  $4i$  (0.588, 0, 0.541), and  $4i$  (0.017, 0, 0.760). Although green phosphorus has the smallest interlayer distance of  $d = 2.16$  Å, the interlayer interaction of 74 meV/atom is comparable to that of black phosphorus (79 meV/atom), indicating that individual layers can be mechanically exfoliated. As the number of atomic layers is reduced to a single layer, the

**Table 1. Lattice Parameters and Energetics of Black, Blue, and Green Phosphorus<sup>a</sup>**

allotrope	bulk					monolayer			
	<i>a</i>	<i>b</i>	<i>c</i>	$\Delta E$	$E_{\text{int}}$	<i>a</i>	<i>b</i>	<i>t</i>	$\Delta E$
blue P	3.29	3.29	3.56	85.7	32.6	3.28	3.28	1.24	1.8
black P	4.44	3.32	3.10	0	79.2	4.62	3.30	2.11	0
	(4.38)	(3.31)	(3.05)						
green P	7.13	7.13	2.16	19.0	73.9	7.27	7.27	2.91	0.9

<sup>a</sup>In-plane lattice constants (*a* and *b* in Å), interlayer spacings (*d* in Å), layer thicknesses (*t* in Å), relative energies ( $\Delta E$  in meV/atom), and interlayer interaction energies ( $E_{\text{int}}$  in meV/atom) are compared for  $\beta$ -P (blue),  $\alpha$ -P (black), and  $\lambda$ -P (green). The PBE-D2 and PBE functionals for the exchange–correlation potential are used for bulk and monolayer structures, respectively. Numbers in parentheses are the experimentally measured values for black phosphorus.<sup>22</sup>

in-plane lattice constants slightly increase from  $a = b = 7.13$  Å to  $a = b = 7.27$  Å (Figure 1). However, the relative stability of the three P allotropes is not affected by forming an isolated monolayer. The energies of green and blue phosphorene relative to black phosphorene are 0.9 and 1.8 meV/atom, respectively. Because these energy differences are extremely small, the energetics of black, blue, and green phosphorene are sensitive to external parameters such as substrate and temperature to be discussed later.

To determine whether green phosphorus maintains its crystal structure under ambient conditions, we examined the phonon spectra of bulk and monolayer green phosphorus and found no imaginary phonon modes over the entire Brillouin zone (BZ) (Figure S2), indicating that both structures are dynamically stable. Similar to blue phosphorus, green phosphorus exhibits more rigid longitudinal optical modes than black phosphorus. The thermal stability of bulk and monolayer green phosphorus was verified by performing *ab initio* molecular dynamics simulations up to 100 ps at a high temperature of 800 K (Figure S2). We also calculated the elastic constants and confirmed that stress–strain relations meet the criteria for mechanical stability in both bulk and monolayer structures (Table S1).

Our results for the electronic structure of green phosphorus are shown in Figure 3a. With the quasiparticle  $G_0W_0$  approximation,<sup>23</sup> we obtained a direct band gap of 0.68 eV at the L point in the BZ for the bulk structure. The fundamental band gap is inversely proportional to the number of atomic layers without altering the direct band gap characteristics. In the monolayer limit, we found a direct band gap of 2.42 eV at the BZ center. This result indicates that green phosphorene is a semiconductor more suitable for electronic and optical applications compared with blue phosphorene with an indirect band gap of 3.34 eV. For green phosphorus in AA stacking, the band gap increases by  $\sim 0.4$  eV and still varies inversely with the number of atomic layers. Similar to black and blue phosphorene, the band gap of green phosphorene is sensitive to strain. The gap size generally decreases under strain, and the band gap nature changes from direct to indirect as strain changes from tensile to compressive (Figure S3).

The optical absorption properties of green phosphorene are investigated by solving the Bethe–Salpeter equation (BSE) together with the quasiparticle  $G_0W_0$  approximation.<sup>24</sup> The inclusion of electron–hole interactions significantly changes the optical properties of green phosphorene. In black phosphorene, the optical absorption spectra are known to be anisotropic, with the stronger exciton effect along the armchair direction,<sup>9</sup> while blue phosphorene exhibits the isotropic absorption spectra (Figure S4). Our  $G_0W_0$ -BSE calculations show the band gap of 1.91 eV and the first absorption peak at 1.20 eV (Table 2). The

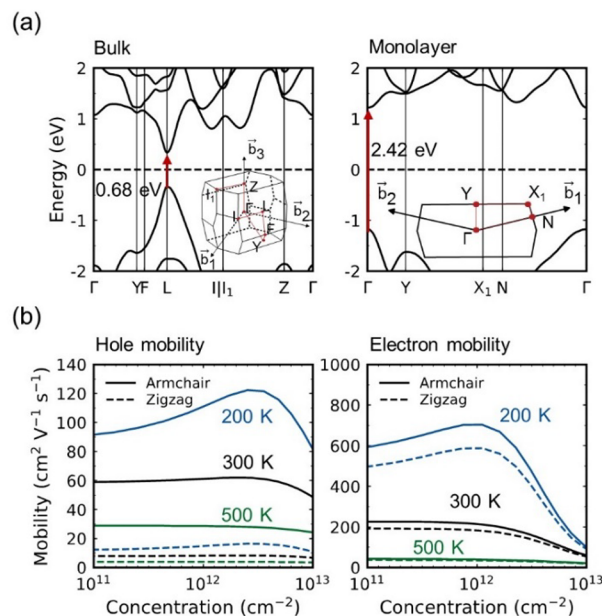


**Figure 3.** (a) Electronic band structures of  $\lambda$ -P (green) in the bulk and monolayer structures using Wannier functions in the quasiparticle  $G_0W_0$  calculations. (b) Hole and electron mobilities of green phosphorene are plotted as a function of carrier concentration along the armchair and zigzag directions, which are defined in Figure 1.

**Table 2. Band Gaps and Exciton Binding Energies of Black, Blue, and Green Phosphorene<sup>a</sup>**

allotrope	$E_g$ (eV)			$E_{\text{ex}}$ (eV)
	PBE	HSE06	$G_0W_0$	$G_0W_0$ -BSE
blue P	1.94 (I)	2.80 (I)	3.34 (I)	1.07
black P	0.90 (D)	1.60 (D)	1.91 (D)	0.71
green P	1.12 (D)	1.86 (D)	2.42 (D)	0.77

<sup>a</sup>Band gaps ( $E_g$ ) and exciton binding energies ( $E_{\text{ex}}$ ) are compared for blue, black, and green phosphorene, based on quasiparticle  $G_0W_0$ , PBE, and hybrid functional (HSE06) calculations for  $E_g$  and  $G_0W_0$ -BSE calculations for  $E_{\text{ex}}$ . Here D and I denote the direct and indirect band gaps, respectively.

exciton binding energy of 710 meV is in good agreement with the previous result of 800 meV.<sup>9</sup> Green phosphorene also shows the anisotropic absorption spectra (Figure S4), with the first peak at 1.65 eV along the armchair direction, and the exciton binding energy at 770 meV, similar to that of black phosphorene. The anisotropic nature of optical absorption spectra implies that green phosphorene is suitable for linear polarizers such as black phosphorene.



Black phosphorene is known to have anisotropic effective masses for both hole and electron carriers, with the higher effective masses along the zigzag direction.<sup>25</sup> In green phosphorene, although the hole effective mass is reduced by about five times along the zigzag direction, it is less affected along the armchair direction, resulting in the strong anisotropy in the hole effective mass (Table S2). On the contrary, because the electron effective mass is reduced by an order of magnitude along the zigzag direction, the nearly isotropic electron mobility is expected.

We calculated electron–phonon coupling matrices using the PBE functional and obtained scattering rates ( $\omega_{n,k}^{\text{el-ph}}$ ) and relaxation times ( $\tau_{n,k}^{\text{el-ph}}$ ) for a band  $n$  and at a wave vector  $\vec{k}$ ,  $\omega_{n,k}^{\text{el-ph}} = \frac{1}{\tau_{n,k}^{\text{el-ph}}} = \frac{2}{\hbar} \text{Im}(\Sigma_{n,k}^{\text{el-ph}})$ , which are related to the imaginary part of electron self-energy  $\text{Im}(\Sigma_{n,k}^{\text{el-ph}})$ .<sup>26,27</sup> The electron and hole mobilities were calculated as a function of carrier concentration by solving the semiclassical Boltzmann equation<sup>28</sup> with the scattering rates  $\omega_{n,k}^{\text{el-ph}}$  (Figure S5). As expected from the analysis of effective masses, green phosphorene exhibits strong anisotropy in hole mobility, while electron mobility is nearly isotropic above room temperature. When temperature is lowered to 200 K, both the hole and electron mobilities increase owing to the suppression of phonon scattering. For carrier concentrations up to  $5 \times 10^{12} \text{ cm}^{-2}$ , the electron mobility is calculated to be  $\sim 200 \text{ cm}^2 \text{ V}^{-1} \text{ s}^{-1}$  at 300 K, which is much higher than the hole mobility of  $\sim 60 \text{ cm}^2 \text{ V}^{-1} \text{ s}^{-1}$  along the armchair direction (Figure 3b and Figure S6). This high electron mobility is attributed to the rapid decrease in scattering rates near the conduction band edge (Figure S5). For black phosphorene, the hole and electron mobilities along the armchair direction are about 150 and  $70 \text{ cm}^2 \text{ V}^{-1} \text{ s}^{-1}$  at 300 K, respectively (Figure S7). While the calculated hole mobility is similar to the previous result of  $170 \text{ cm}^2 \text{ V}^{-1} \text{ s}^{-1}$ ,<sup>29</sup> it was experimentally reported that the hole mobility varies from about 200 to  $50 \text{ cm}^2 \text{ V}^{-1} \text{ s}^{-1}$  as the film thickness decreases to a few layers.<sup>7</sup> On the contrary, the scattering rates of blue phosphorene are higher near the valence band edge than those of black and green phosphorene. Therefore, blue phosphorene shows an extremely low mobility of 0.1 to  $0.2 \text{ cm}^2 \text{ V}^{-1} \text{ s}^{-1}$  for hole carriers as compared with the electron mobility of  $5\text{--}10 \text{ cm}^2 \text{ V}^{-1} \text{ s}^{-1}$  (Figure S8). On the basis of the results, it is inferred that green phosphorene can serve as a potential material for  $n$ -type devices due to its high electron mobility.

The effect of temperature on the relative stability of black, blue, and green phosphorene was studied by calculating the Helmholtz free energy that includes both the vibrational entropy and zero-point energy. Our calculations show that blue phosphorene becomes more stable than black phosphorene above 143 K, consistent with the previous result of 135 K, which was based on the Gibbs free energy.<sup>30</sup> However, we note that blue phosphorene is always metastable with respect to green phosphorene for temperatures up to 300 K. In fact, black phosphorene is more likely to transform to green phosphorene at a lower temperature of 87 K (Figure 4a). We considered a possible transition pathway from black to green phosphorene, which is accompanied by bond breaking and rebonding relaxations (Figure S9). Using the nudged elastic band (NEB) method, we estimated the energy barrier to be 0.21 eV/atom (Figure 4b), lower than the previously reported barrier of 0.47 eV/atom for the transition from black to blue

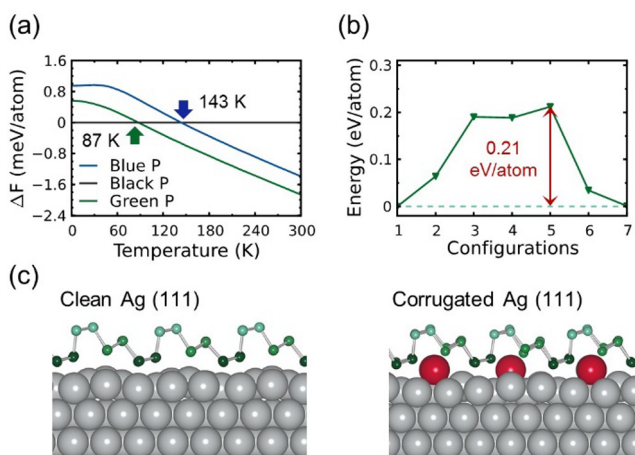


**Figure 4.** (a) Helmholtz free energies ( $\Delta F$ ) of blue and green phosphorene relative to black phosphorene are plotted as a function of temperature, with neglecting the thermal expansion effect. (b) Total energy variation is drawn during the transformation from black to green phosphorene (Figure S9). (c) Atomic structures of green phosphorene on clean and corrugated Ag(111) surfaces are drawn. It is energetically more probable to synthesize green phosphorene on the corrugated surface. Red balls represent the periodically corrugated Ag atoms.

phosphorene.<sup>13</sup> In the NEB method, we considered concerted motions for a finite-size supercell geometry due to computational limitations. In the previous study for graphite-to-diamond phase transition,<sup>31</sup> the transition barriers were shown to be lower for nucleation processes than for concerted pathways. Thus the NEB value represents the upper limit of the transition barrier from black to green phosphorene. The sizable kinetic energy barrier for the conversion to green phosphorene can be overcome using a laser-driven phase patterning technique.<sup>32</sup>

We also examined the stability of the three allotropes on metal substrates including Al, Au, and Ag (Table S3). Blue phosphorene is the most favorable allotrope on the clean (111) surfaces of Au and Ag, while black phosphorene is more stable on the Al substrate. The energetics of blue phosphorene is in good agreement with the recent experimental realization on the Au substrate.<sup>19</sup> On the contrary, green phosphorene is well-matched to wrinkled surfaces due to its buckled structure, as shown in Figure 4c. Thus green phosphorene has the lowest formation energy on the corrugated (111) surfaces of Au and Ag (Table S3), indicating that this new allotrope can be realized on corrugated metal surfaces.

In conclusion, we have predicted a novel P allotrope called green phosphorus using an evolutionary crystal structure search method. The structure of green phosphorus is characterized by a combination of blue and black phosphorus, and its stability is confirmed from the phonon spectra and molecular dynamics simulations. While blue phosphorus has indirect band gaps, green phosphorus exhibits direct band gap characteristics, regardless of the number of atomic layers. The band gap sizes are tunable in the visible range by varying the film thickness, lying in between black and blue phosphorus. Because of the strong anisotropy in the optical and transport properties, a monolayer of green phosphorus, termed green phosphorene, is promising for novel 2D devices employing anisotropic properties. Furthermore, our calculations suggest that the transition from black to green phosphorene can occur at

temperatures above 87 K, and the synthesis of green phosphorene is possible on corrugated metal substrates, making the boundary of phosphorus-based applications go beyond black phosphorus.

## CALCULATION METHODS

The structural optimization and electronic structure calculations were performed using the functional form proposed by Perdew, Burke, and Ernzerhof (PBE)<sup>33</sup> for the exchange-correlation potential within the framework of density functional theory and the projector augmented wave potentials,<sup>34</sup> as implemented in the VASP code.<sup>35</sup> To describe more accurately interlayer interactions, we additionally used the PBE-D2 functional, which includes van der Waals forces,<sup>36</sup> yielding the lattice constants (Table 1) in good agreement with the experimentally measured values for black phosphorus.<sup>22</sup> The wave functions were expanded in plane waves up to an energy cutoff of 500 eV. For Brillouin zone integration, we used the *k*-point sets generated by the  $16 \times 16 \times 1$  and  $12 \times 12 \times 12$  Monkhorst–Pack meshes for 2D and 3D systems, respectively. The ionic coordinates were fully optimized until the residual forces and stress tensors were less than 0.01 eV/Å and 1.5 kbar, respectively.

The dynamical matrices were calculated by using a finite difference method, as implemented in the Phonopy code,<sup>37</sup> and used to obtain the full phonon spectra. Using the vibrational spectra, the vibrational entropies, specific heats at constant volume, and Helmholtz free energies were calculated for blue, black, and green phosphorene. The scattering rates for electrons are originated from electron–phonon interactions. The electron–phonon matrices were calculated by using the PBE exchange–correlation functional and the norm-conserving pseudopotentials within the density functional perturbation theory, as implemented in the QUANTUM ESPRESSO code.<sup>38</sup> The calculated matrices for the  $10 \times 10 \times 1$  *k* and  $10 \times 10 \times 1$  *q* meshes were interpolated to the  $100 \times 100 \times 1$  *k* and  $100 \times 100 \times 1$  *q* meshes, respectively, using a Wannier function interpolation scheme in the EPW package.<sup>26,27</sup>

## ASSOCIATED CONTENT

### Supporting Information

The Supporting Information is available free of charge on the ACS Publications website at DOI: 10.1021/acs.jpclett.7b02153.

Calculation details, metastable P allotropes, dynamical and thermal stability, band gap variation with strain, optical absorption spectra, scattering rates from electron–phonon interaction, mobility, transition pathway from black to green phosphorene, X-ray diffraction spectra, STM images, elastic constants, effective masses, and formation energies on metal substrates are included. (PDF)

## AUTHOR INFORMATION

### Corresponding Author

\*E-mail: kjchang@kaist.ac.kr.

### ORCID

Sunghyun Kim: 0000-0001-5072-6801

Kee Joo Chang: 0000-0002-5364-8551

### Present Address

§S.K.: Department of Materials, Imperial College London, London SW7 2AZ, U.K.

## Notes

The authors declare no competing financial interest.

## ACKNOWLEDGMENTS

W.H.H. thanks Dr. Seoung-Hun Kang and Mr. Seungjun Lee for useful discussions on EPW. This work was supported by Samsung Science and Technology Foundation under Grant No. SSTFBA1401-08.

## REFERENCES

- (1) Novoselov, K. S.; Geim, A. K.; Morozov, S. V.; Jiang, D.; Zhang, Y.; Dubonos, S. V.; Grigorieva, I. V.; Firsov, A. A. Electric field effect in atomically thin carbon films. *Science* **2004**, *306*, 666–669.
- (2) Geim, A. K.; Grigorieva, I. V. Van der Waals heterostructures. *Nature* **2013**, *499*, 419–425.
- (3) Novoselov, K. S.; Geim, A. K.; Morozov, S.; Jiang, D.; Katsnelson, M.; Grigorieva, I.; Dubonos, S.; Firsov, A. Two-dimensional gas of massless Dirac fermions in graphene. *Nature* **2005**, *438*, 197–200.
- (4) Zhang, Y.; Tan, Y.-W.; Stormer, H. L.; Kim, P. Experimental observation of the quantum Hall effect and Berry's phase in graphene. *Nature* **2005**, *438*, 201–204.
- (5) Yang, H.; Heo, J.; Park, S.; Song, H. J.; Seo, D. H.; Byun, K.-E.; Kim, P.; Yoo, I.; Chung, H.-J.; Kim, K. Graphene barristor, a triode device with a gate-controlled Schottky barrier. *Science* **2012**, *336*, 1140–1143.
- (6) Ling, X.; Wang, H.; Huang, S.; Xia, F.; Dresselhaus, M. S. The renaissance of black phosphorus. *Proc. Natl. Acad. Sci. U. S. A.* **2015**, *112*, 4523–4530.
- (7) Liu, H.; Neal, A. T.; Zhu, Z.; Luo, Z.; Xu, X.; Tománek, D.; Ye, P. D. Phosphorene: an unexplored 2D semiconductor with a high hole mobility. *ACS Nano* **2014**, *8*, 4033–4041.
- (8) Li, L.; Yu, Y.; Ye, G. J.; Ge, Q.; Ou, X.; Wu, H.; Feng, D.; Chen, X. H.; Zhang, Y. Black phosphorus field-effect transistors. *Nat. Nanotechnol.* **2014**, *9*, 372–377.
- (9) Tran, V.; Soklaski, R.; Liang, Y.; Yang, L. Layer-controlled band gap and anisotropic excitons in few-layer black phosphorus. *Phys. Rev. B: Condens. Matter Mater. Phys.* **2014**, *89*, 235319.
- (10) Li, L.; Kim, J.; Jin, C.; Ye, G. J.; Qiu, D. Y.; da Jornada, F. H.; Shi, Z.; Chen, L.; Zhang, Z.; Yang, F.; et al. Direct observation of the layer-dependent electronic structure in phosphorene. *Nat. Nanotechnol.* **2016**, *12*, 21–25.
- (11) Qiao, J.; Kong, X.; Hu, Z.-X.; Yang, F.; Ji, W. High-mobility transport anisotropy and linear dichroism in few-layer black phosphorus. *Nat. Commun.* **2014**, *5*, 4475.
- (12) Wang, H.; Wang, X.; Xia, F.; Wang, L.; Jiang, H.; Xia, Q.; Chin, M. L.; Dubey, M.; Han, S.-j. Black phosphorus radio-frequency transistors. *Nano Lett.* **2014**, *14*, 6424–6429.
- (13) Zhu, Z.; Tománek, D. Semiconducting layered blue phosphorus: a computational study. *Phys. Rev. Lett.* **2014**, *112*, 176802.
- (14) Guan, J.; Zhu, Z.; Tománek, D. High stability of faceted nanotubes and fullerenes of multiphase layered phosphorus: A computational study. *Phys. Rev. Lett.* **2014**, *113*, 226801.
- (15) Zhao, T.; He, C.; Ma, S.; Zhang, K.; Peng, X.; Xie, G.; Zhong, J. A new phase of phosphorus: the missed tricycle type red phosphorene. *J. Phys.: Condens. Matter* **2015**, *27*, 265301.
- (16) Wu, M.; Fu, H.; Zhou, L.; Yao, K.; Zeng, X. C. Nine new phosphorene polymorphs with non-honeycomb structures: a much extended family. *Nano Lett.* **2015**, *15*, 3557–3562.
- (17) Schusteritsch, G.; Uhrin, M.; Pickard, C. J. Single-Layered Hittorf's Phosphorus: A Wide-Bandgap High Mobility 2D Material. *Nano Lett.* **2016**, *16*, 2975–2980.
- (18) Wang, H.; Li, X.; Liu, Z.; Yang, J. *ψ*-Phosphorene: a new allotrope of phosphorene. *Phys. Chem. Chem. Phys.* **2017**, *19*, 2402–2408.
- (19) Zhang, J. L.; Zhao, S.; Han, C.; Wang, Z.; Zhong, S.; Sun, S.; Guo, R.; Zhou, X.; Gu, C. D.; Yuan, K. D.; et al. Epitaxial growth of single layer blue phosphorus: a new phase of two-dimensional phosphorus. *Nano Lett.* **2016**, *16*, 4903–4908.

- (20) Lee, I.-H.; Oh, Y. J.; Kim, S.; Lee, J.; Chang, K. J. *Ab initio* materials design using conformational space annealing and its application to searching for direct band gap silicon crystals. *Comput. Phys. Commun.* **2016**, *203*, 110–121.
- (21) Bachhuber, F.; von Appen, J.; Dronsowski, R.; Schmidt, P.; Nilges, T.; Pfitzner, A.; Weihrich, R. The extended stability range of phosphorus allotropes. *Angew. Chem., Int. Ed.* **2014**, *53*, 11629–11633.
- (22) Brown, A.; Rundqvist, S. Refinement of the crystal structure of black phosphorus. *Acta Crystallogr.* **1965**, *19*, 684–685.
- (23) Hybertsen, M. S.; Louie, S. G. Electron correlation in semiconductors and insulators: Band gaps and quasiparticle energies. *Phys. Rev. B: Condens. Matter Mater. Phys.* **1986**, *34*, 5390–5413.
- (24) Rohlfing, M.; Louie, S. G. Electron-hole excitations and optical spectra from first principles. *Phys. Rev. B: Condens. Matter Mater. Phys.* **2000**, *62*, 4927–4944.
- (25) Wang, L.; Kutana, A.; Zou, X.; Yakobson, B. I. Electro-mechanical anisotropy of phosphorene. *Nanoscale* **2015**, *7*, 9746–9751.
- (26) Giustino, F.; Cohen, M. L.; Louie, S. G. Electron-phonon interaction using Wannier functions. *Phys. Rev. B: Condens. Matter Mater. Phys.* **2007**, *76*, 165108.
- (27) Poncé, S.; Margine, E. R.; Verdi, C.; Giustino, F. EPW: Electron–phonon coupling, transport and superconducting properties using maximally localized Wannier functions. *Comput. Phys. Commun.* **2016**, *209*, 116–133.
- (28) Pizzi, G.; Volja, D.; Kozinsky, B.; Fornari, M.; Marzari, N. BoltzWann: A code for the evaluation of thermoelectric and electronic transport properties with a maximally-localized Wannier functions basis. *Comput. Phys. Commun.* **2014**, *185*, 422–429.
- (29) Liao, B.; Zhou, J.; Qiu, B.; Dresselhaus, M. S.; Chen, G. *Ab initio* study of electron-phonon interaction in phosphorene. *Phys. Rev. B: Condens. Matter Mater. Phys.* **2015**, *91*, 235419.
- (30) Aierken, Y.; Çakır, D.; Sevik, C.; Peeters, F. M. Thermal properties of black and blue phosphorenes from a first-principles quasiharmonic approach. *Phys. Rev. B: Condens. Matter Mater. Phys.* **2015**, *92*, 081408.
- (31) Khaliullin, R. Z.; Eshet, H.; Kühne, T. D.; Behler, J.; Parrinello, M. Nucleation mechanism for the direct graphite-to-diamond phase transition. *Nat. Mater.* **2011**, *10*, 693–697.
- (32) Cho, S.; et al. Phase patterning for ohmic homojunction contact in MoTe<sub>2</sub>. *Science* **2015**, *349*, 625–628.
- (33) Perdew, J. P.; Burke, K.; Ernzerhof, M. Generalized gradient approximation made simple. *Phys. Rev. Lett.* **1996**, *77*, 3865–3868.
- (34) Blöchl, P. E. Projector augmented-wave method. *Phys. Rev. B: Condens. Matter Mater. Phys.* **1994**, *50*, 17953–17979.
- (35) Kresse, G.; Furthmüller, J. Efficient iterative schemes for *ab initio* total-energy calculations using a plane-wave basis set. *Phys. Rev. B: Condens. Matter Mater. Phys.* **1996**, *54*, 11169–11186.
- (36) Grimme, S. Semiempirical GGA-type density functional constructed with a long-range dispersion correction. *J. Comput. Chem.* **2006**, *27*, 1787–1799.
- (37) Togo, A.; Tanaka, I. First principles phonon calculations in materials science. *Scr. Mater.* **2015**, *108*, 1–5.
- (38) Giannozzi, P.; et al. QUANTUM ESPRESSO: a modular and open-source software project for quantum simulations of materials. *J. Phys.: Condens. Matter* **2009**, *21*, 395502.